

Elucidation of homojunction formation in CuInS_2 with impedance spectroscopy

Ruben Loeff^(a),b)

Opto-Electronic Materials, Delft University of Technology, Julianalaan 136, 2628 BL Delft, The Netherlands

Joop Schoonman

Delft Institute for Sustainable Energy, Delft University of Technology, Julianalaan 136, 2628 BL Delft, The Netherlands

Albert Goossens^{b)}

Opto-Electronic Materials, Delft University of Technology, Julianalaan 136, 2628 BL Delft, The Netherlands

(Received 8 February 2007; accepted 6 June 2007; published online 26 July 2007)

Type transformation in CuInSe_2 and CuInS_2 solar cells is an important issue with far reaching consequences. In the present study, the presence of a p - n homojunction inside CuInS_2 in a $\text{TiO}_2/\text{CuInS}_2$ device is revealed with a detailed impedance spectroscopy and capacitance study. A n -type CuInS_2 film with a thickness of 40 nm is found at the TiO_2 (n -type)/ CuInS_2 (p -type) interface. The effective donor density of this n -type film is $2 \times 10^{17} \text{ cm}^{-3}$ at 400 K and is higher than the effective acceptor density in the remaining p -type CuInS_2 , being $4 \times 10^{16} \text{ cm}^{-3}$ at 400 K. Both densities decrease upon increasing the temperature. This is explained by the activation of a Cu_{In}'' acceptor state in n -type CuInS_2 and a thermally activated hole trap in p -type CuInS_2 . © 2007 American Institute of Physics. [DOI: [10.1063/1.2759470](https://doi.org/10.1063/1.2759470)]

I. INTRODUCTION

Chalcopyrite semiconductors have attracted widespread attention for use in thin-film solar cells.^{1–4} CuInS_2 has a high absorption coefficient of $1 \times 10^5 \text{ cm}^{-1}$ at 500 nm,⁵ and a direct band gap of 1.5 eV, which matches well with the solar spectrum.⁶ To date, efficiencies up to 19% are obtained with chalcopyrite-based solar cells.⁷ Unfortunately, the most efficient chalcopyrite-based solar cell configurations contain the toxic components Cd and Se. In our configuration, instead of CdS, TiO_2 is used as the n -type component. In recent years, the use of ZnO buffer has been introduced. However, in the spray pyrolysis deposition method, which is used to prepare the samples, the application of TiO_2 instead of ZnO gives better results. TiO_2 and ZnO have approximately the same valence and conduction band positions, which allow the use of TiO_2 as electron accepting material.⁸ Furthermore, an $\text{In}_2(\text{S},\text{Se})_3$ buffer layer can be used instead of Cd(S,Se). Nanu *et al.* reported efficiencies up to 4% for $\text{TiO}_2/\text{CuInS}_2$ solar cells, without buffer layer.⁹ Furthermore, these cells can be produced on a large scale, using low-cost deposition techniques, with efficiencies up to 7%.¹⁰ Nevertheless, the efficiency still needs to be improved, which is a strong incentive to investigate the defect chemistry of CuInS_2 in depth. Charge carrier densities between 10^{17} and 10^{18} cm^{-3} have been found with capacitance studies on chalcopyrite-based solar cells.^{11–13} In this paper, the defect chemistry of CuInS_2 is studied by measuring the temperature dependence of the space-charge capacitance in $\text{TiO}_2/\text{CuInS}_2$ devices.^{9,14,15} With

this approach, we are able to elucidate the effective carrier densities and the widths of the depletion regions in n -type TiO_2 and p -type CuInS_2 . Furthermore, we provide evidence for the presence of a 40 nm thin interfacial n -type region in CuInS_2 between n -type TiO_2 and p -type CuInS_2 , i.e., homojunction formation. The presence of this n -type layer is expected to be independent of the metal oxide layer used. Furthermore, when the mechanism of the formation of the n -type layer can be controlled, the need of a CdS or In_2S_3 buffer layer may disappear.

The study of homojunction formation in chalcopyrite crystals dates back to the 1970s. In these studies, semiconductor-type transformation at the interface of CuInSe_2 crystals have been stimulated by applying specific annealing conditions. n - to p -type transformation is observed when annealing CuInS_2 or CuInSe_2 at high temperatures ($>650 \text{ }^\circ\text{C}$) in S or Se vapor, respectively. p to n transformations are observed after annealing the Zn, Cd, In, or Cu plated p -type samples at $T > 200 \text{ }^\circ\text{C}$, and after annealing in Cd vapor at $400 \text{ }^\circ\text{C}$ or Cd-ion implantation.^{16–22}

In 1974, Wagner *et al.* introduced the first CdS/ CuInSe_2 photovoltaic detector²³ and the first chalcopyrite-based solar cells are obtained in 1975 and 1977.^{24,25} Type transformation of CuInSe_2 also occurs in CdS/ CuInSe_2 solar cells after CdS deposition on both single crystal and thin-film CuInSe_2 . Type transformation in single crystals is probably caused by Cd diffusion in CuInSe_2 , leading to a homojunction in CuInSe_2 instead of the expected heterojunction.^{26–30} In thin-film devices, the origin of this phenomenon is assigned to the presence of a Cu-poor surface defect layer at the CdS interface.^{31–34} In 1992, Cahen *et al.* showed that it is also possible to create a homojunction in CuInSe_2 by applying a

^{a)}FAX: +31-182787421; electronic mail: r.loef@tudelft.nl

^{b)}Also at Delft Institute for Sustainable Energy, Delft University of Technology, Julianalaan 136, 2628 BL Delft, The Netherlands.

strong electric field on the samples at room temperature.^{12,35,36} In the studies described above, the presence of a homojunction in CuInSe₂ has been detected with electron-beam-induced current (EBIC) and secondary ion-mass spectroscopy (SIMS). With these techniques only thick type-converted CuInSe₂ layers (several micrometers) can be observed.

Less is known about this phenomenon in CuInS₂, especially not for the CuInS₂/TiO₂ combination of the present investigation. By using impedance spectroscopy, we have been able to monitor the presence of a *n*-type region in CuInS₂ with unprecedented accuracy. The thickness, as well as the effective donor and acceptor densities, has been determined. Furthermore, by measuring the temperature dependence of the interface capacitance, the energy positions of the involved deep acceptor state and deep hole trap have been found.

II. EXPERIMENTAL ASPECTS

Flat anatase *n*-type TiO₂ and Cu-rich *p*-type CuInS₂ films are subsequently deposited by spray pyrolysis on transparent conductive oxide (TCO) glass substrates (SnO₂:F, Libbey Owens Ford, TEC-18). More information about the spray deposition of CuInS₂ and TiO₂ has been published previously.^{37,38} Circular carbon spots (diameter of 2.3 mm) are applied onto CuInS₂ as back contact (graphite conductive adhesive, aqueous based, Alfa Aesar). TiO₂ without CuInS₂ layers are analyzed in 0.1M KOH electrolyte, with a Ag/AgCl reference electrode. Current-voltage (*J*- ϕ) measurements are recorded with a Princeton Applied Research potentiostat (PAR283). For impedance spectroscopy (IS) and capacitance-voltage (*C*- ϕ) measurements, a frequency response analyzer (Schlumberger FRA 1255) is added. For IS measurements, an ac voltage of 10 mV is applied in a frequency range of 100 Hz–1 MHz in addition to a dc bias. The TiO₂/CuInS₂ samples are mounted in a nitrogen atmosphere in a N₂ cryostat (Oxford Instruments Optistat DN). *J*- ϕ , IS, and *C*- ϕ data are measured in the temperature range of 300–500 K. All experiments are performed in the dark. A Veeco Dektak 8 surface profiler is used for layer thickness determination.

III. RESULTS AND DISCUSSION

J- ϕ measurements in the dark show good diode behavior at all temperatures, as shown in Fig. 1. Impedance spectra at different potentials and temperatures are presented in Fig. 2. The equivalent circuit, shown in Fig. 3, represents the frequency response between 100 Hz and 1 MHz adequately. Nonlinear least squares fitting of the equivalent circuit elements to the impedance spectra gives excellent results for all temperatures. At frequencies above 10 kHz, the fits have a relative error of less than 4%. In the equivalent circuit, *R*₁ represents the series resistance, *R*₂ the shunt resistance, *C*₁ the space-charge capacitance, and the *R*₃-CPE₁ branch the trapping of charge carriers in deep states. For frequencies above 100 kHz, the *R*₁*C*₁ branch dominates over the others, i.e., $\tau_{R_1 C_1} \ll \tau_{R_3-CPE_1}$. Accordingly, at 1 MHz *C*₁, being the space-charge capacitance, can be calculated directly from the

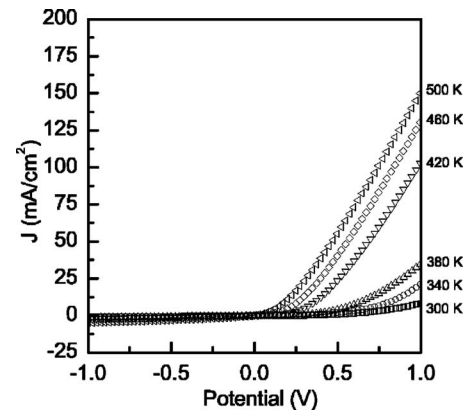


FIG. 1. *J*- ϕ curves of TiO₂/CuInS₂ devices at different temperatures in the dark.

imaginary part of the impedance *Z*'. Comparing the *C*₁ values obtained from fitting and that from *Z*' at 1 MHz indeed shows good agreement. For instance, at *T*=400 K and $\phi = 0$ V *C*₁=2.4 nF obtained from fitting and 2.7 nF when calculating from *Z*' at 1 MHz. Upon constructing a Mott-Schottky plot of *C*₁⁻² vs ϕ , the obtained slopes and transition voltages (to be discussed below) are not affected by the small overestimation of the space-charge capacitance at 1 MHz.

Figure 4 shows Mott-Schottky *C*⁻²- ϕ plots recorded at 1 MHz at different temperatures. All transition voltages and slopes are summarized in the supplemental material.³⁹ At high temperatures (*T*>340 K) three slopes are observed, while at low temperatures (*T*<340 K) only two slopes are found. To distinguish between the different regions (i.e., slopes) in the *C*⁻²- ϕ plots, we first determine the properties of the TiO₂ and TCO films. Impedance analysis and *C*- ϕ profiling on TCO/TiO₂ samples is performed in a KOH electrolyte to ensure a well-defined Schottky contact. Figure 5 shows the results of a *C*- ϕ measurement on a TCO/TiO₂ sample recorded at 10 kHz. Donor densities of 2×10^{17} and 2×10^{20} cm⁻³ are found for TiO₂ and TCO, respectively. TiO₂ has a film thickness of 140 nm, which is in excellent agreement with surface profiler measurements. Upon combining these results with the *C*⁻²- ϕ plots of TiO₂/CuInS₂ devices with solid contacts, the slope at $\phi < -0.5$ V corresponds well with that of TiO₂. The situation where TCO is dominant is never found, which implies that between 300 and 500 K at -1 V, TiO₂ is not in full depletion.

First, the *C*⁻²- ϕ behavior at high temperatures is discussed. For $\phi > -0.5$ V two slopes are left unassigned, which means that in addition to TiO₂, at least two other space-charge regions must be present, both located in the CuInS₂ film. It is known that due to copper diffusion the conductivity of CuInS₂ can change from *p* type to *n* type.^{40,41} We also have taken into account the possibility of Cu migration into TiO₂, although it is rather unlikely that the positively charged Cu ions will migrate against the electric field toward the TiO₂. Cu diffusion into TiO₂ yields Cu_i^{*} donor states, which leads to an increase of the donor density at the TiO₂ surface region. However, a TiO₂ region with *N*_D> 2×10^{17} cm⁻³ is not observed. Therefore, we conclude that between *p*-type CuInS₂ (*p*-CuInS₂) and *n*-type TiO₂ (*n*-TiO₂) a *n*-type CuInS₂ (*n*-CuInS₂) layer is formed during

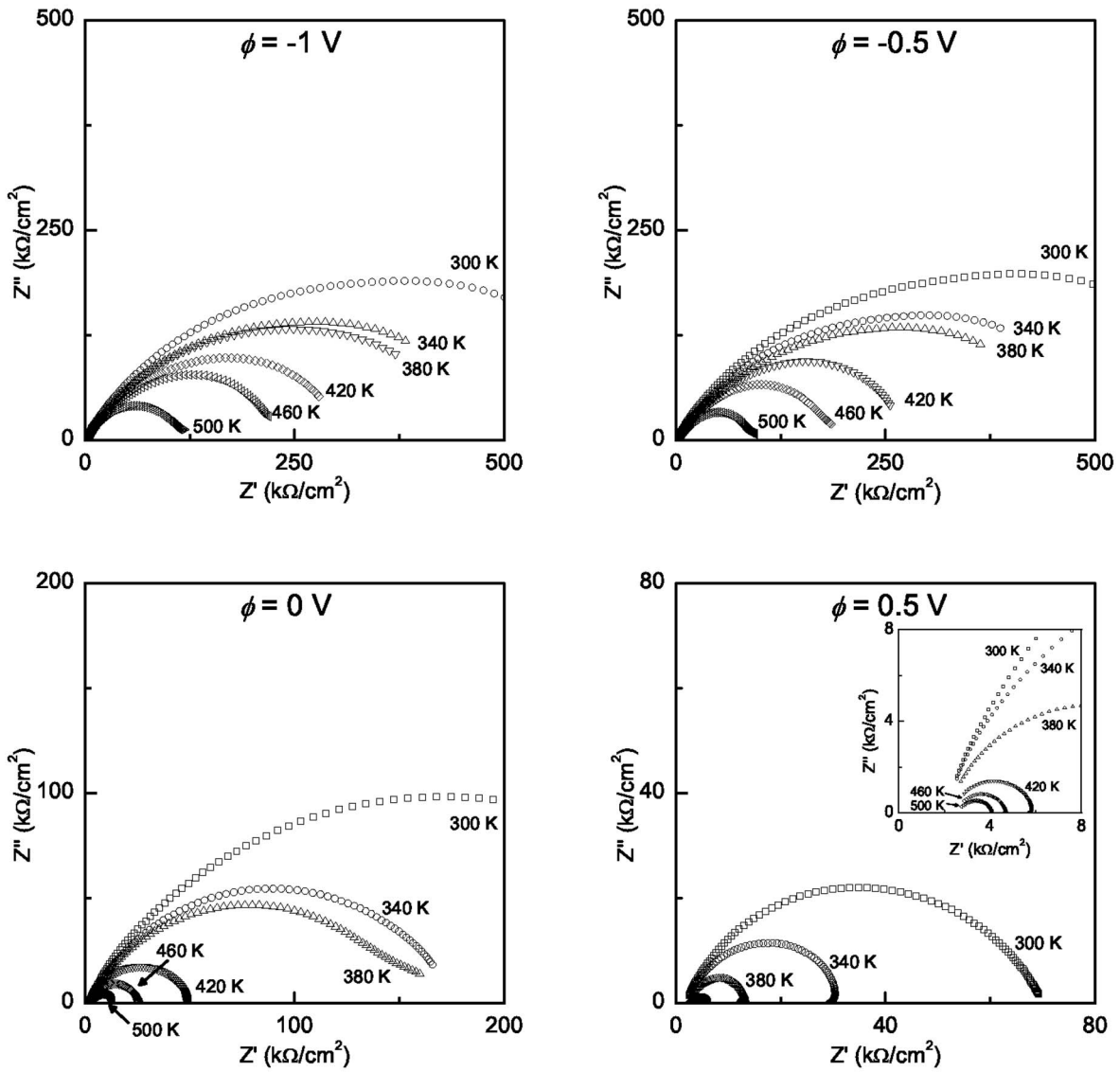


FIG. 2. Impedance spectra of TiO₂/CuInS₂ devices at different potentials and temperatures. At $\phi=0.5$ V the high-frequency regime is magnified in the inset.

the deposition and annealing. With a *p-n* homojunction inside the CuInS₂ film, the device is now modeled as a *p-n-n* system (*p*-CuInS₂/*n*-CuInS₂/*n*-TiO₂). Both CuInS₂ layers are in full depletion at $\phi < -0.5$ V, as shown in Fig. 6-I. The situation at 0 V < $\phi < 0.5$ V, close to the flatband situation, is presented in Fig. 7. Now, the sample is described by a *p-n* homojunction inside CuInS₂ with no electric field present in TiO₂ because this is the junction where *p*-type and *n*-type

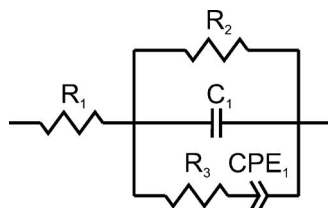


FIG. 3. Equivalent circuit for a TiO₂/CuInS₂ device. R_1 represents the series resistance, R_2 the shunt resistance, and C_1 the space-charge capacitance. The low frequency R_3 - CPE_1 branch represents charge trapping in deep states.

materials meet. At the intermediate voltage region -0.5 V < $\phi < 0$ V, only one of the CuInS₂ regions (*n* or *p*) has reached full depletion. Model A (II-A) considers a fully depleted *n*-CuInS₂ layer, while model B (II-B) considers a fully depleted *p*-CuInS₂ layer. Both possibilities are modeled with the mathematical analysis given in the supplemental information.³⁹

The local electric field E is calculated by integration of the Gauss equation. We assume homogeneous donor and acceptor concentrations in the *n*-type and *p*-type CuInS₂ regions, respectively. The potential drop over the layers is calculated from integrating the electric field. When a potential ϕ falls across the depletion region in the sample, the capacitance C of the sample is given by

$$C = \frac{dQ_n}{d\phi} = \frac{dQ_p}{d\phi}. \tag{1}$$

Here, Q is the charge in the depletion layer. Interface and surface states are not included in our model. The complete

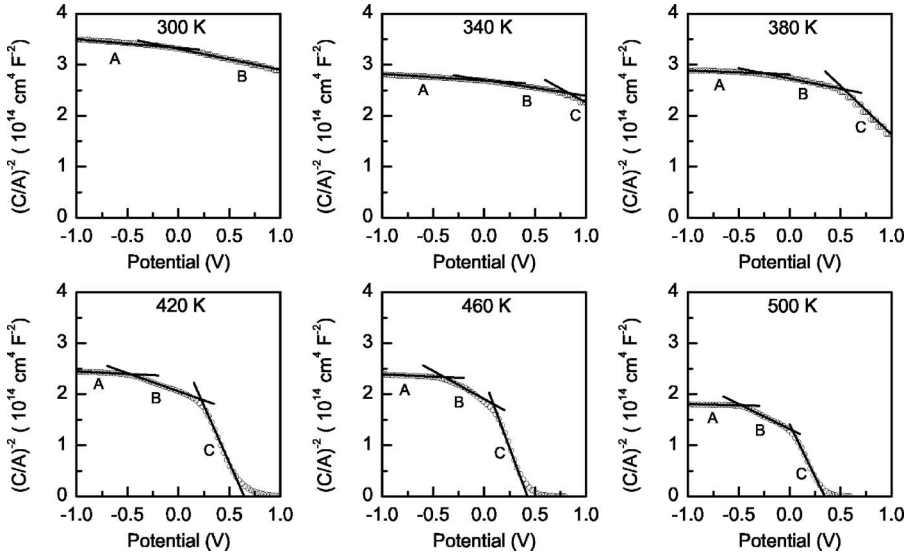


FIG. 4. C^{-2} - ϕ plots of a TCO/TiO₂/CuInS₂/carbon device at different temperatures. The values of slopes A, B, and C and their transition points are summarized in the supplemental material.

mathematical analysis can be found in the supplemental material³⁹ and the final results are summarized here. The situation of Fig. 6-I, in which both CuInS₂ layers are in full depletion, leads to

$$\frac{1}{C^2} = \left(1 + \frac{\epsilon_{\text{CIS}} N_{A,p\text{-CIS}}}{\epsilon_{\text{TiO}_2} N_{D,\text{TiO}_2}} \right) \left(\frac{w_{p\text{-CIS}}}{\epsilon_{\text{CIS}}} \right)^2 + \left(1 - \frac{\epsilon_{\text{CIS}} N_{D,n\text{-CIS}}}{\epsilon_{\text{TiO}_2} N_{D,\text{TiO}_2}} \right) \times \left[\left(\frac{w_{n\text{-CIS}}}{\epsilon_{\text{CIS}}} \right)^2 + 2 \frac{w_{n\text{-CIS}} w_{p\text{-CIS}}}{\epsilon_{\text{CIS}}^2} \right] + \frac{2}{q \epsilon_{\text{TiO}_2} N_{D,\text{TiO}_2}} \phi. \quad (2)$$

Here, ϵ is the dielectric constant, q is the electron charge, N is the ionized donor or acceptor density, and w is the layer thickness.

When n -CuInS₂ is fully depleted, model A (Fig. 6-II-A) holds, leading to the following equation:

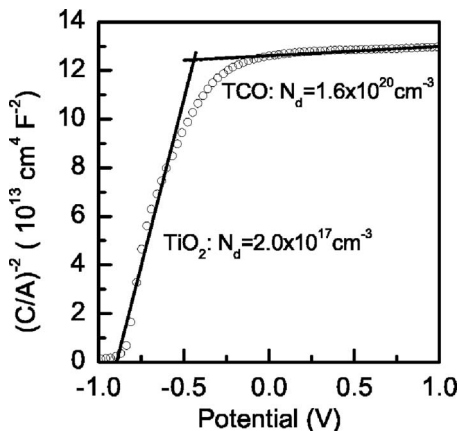


FIG. 5. C^{-2} - ϕ plots of a TCO/TiO₂ electrode in a KOH electrolyte. Donor densities of both TCO and TiO₂ are calculated from the two slopes. Dielectric constants of 3.7 and 55 are used for TCO and anatase TiO₂, respectively.

$$\frac{1}{C^2} = \left(1 + \frac{N_{D,n\text{-CIS}}}{N_{A,p\text{-CIS}}} \right) \left(1 - \frac{\epsilon_{\text{CIS}} N_{D,n\text{-CIS}}}{\epsilon_{\text{TiO}_2} N_{D,\text{TiO}_2}} \right) \frac{w_{n\text{-CIS}}^2}{\epsilon_{\text{CIS}}^2} + \frac{2(\epsilon_{\text{CIS}} N_{D,p\text{-CIS}} + \epsilon_{\text{TiO}_2} N_{D,\text{TiO}_2})}{q \epsilon_{\text{TiO}_2} \epsilon_{\text{CIS}} N_{D,\text{TiO}_2} N_{A,p\text{-CIS}}} \phi. \quad (3)$$

When p -CuInS₂ is fully depleted, model B (Fig. 6-II-B) holds, i.e.,

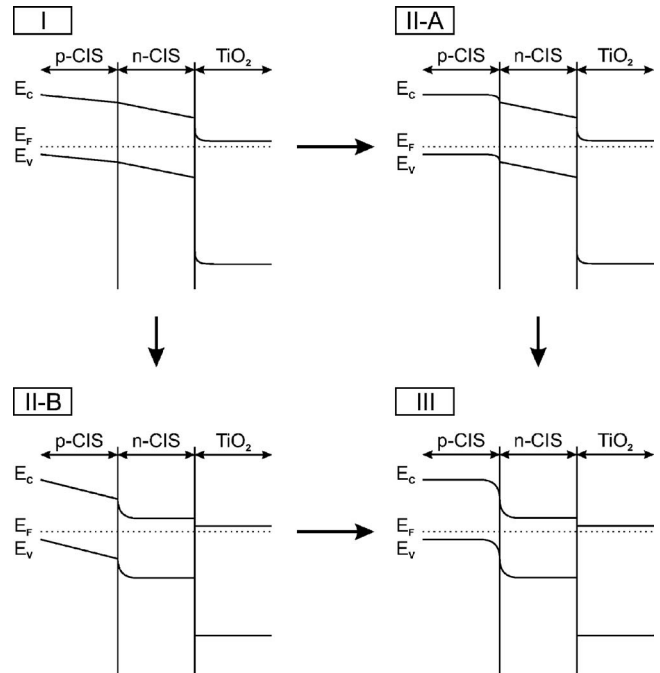


FIG. 6. Band diagrams of p -CuInS₂/ n -CuInS₂/ n -TiO₂ as a function of temperature at zero applied bias voltage. Situation I: $T < 340$ K; n - and p -type CuInS₂ are both in full depletion. Situations IIA and IIB: $340 < T < 400$ K; either n -CuInS₂ is fully depleted (model A) or p -CuInS₂ is fully depleted (model B). Situation III: $T > 400$ K; neither n -CuInS₂ nor p -CuInS₂ is in full depletion.

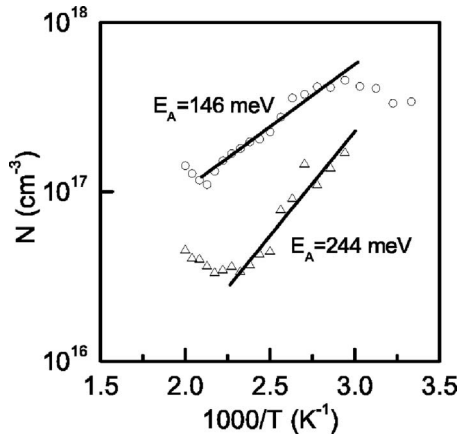


FIG. 7. Effective donor density in n -CuInS₂ (○), and acceptor density in p -CuInS₂ (△) in a TiO₂/ n -CuInS₂/ p -CuInS₂ heterojunction following model B.

$$\frac{1}{C^2} = \left(1 + \frac{N_{A,p-CIS}}{N_{D,n-CIS}}\right) \left(\frac{w_{p-CIS}}{\epsilon_{CIS}}\right)^2 + \frac{2}{q\epsilon_{CIS}N_{D,n-CIS}}\phi. \quad (4)$$

Finally, close to the flatband situation, the well-known C^{-2} - ϕ equation for p - n junctions is valid,

$$\frac{1}{C^2} = \frac{2(\epsilon_{CuInS_2}N_{D,n-CuInS_2} + \epsilon_{CuInS_2}N_{A,p-CuInS_2})\phi}{q\epsilon_{CuInS_2}^2N_{D,n-CuInS_2}N_{A,p-CuInS_2}}. \quad (5)$$

Upon fitting the above expressions to the experimental data, using relative dielectric constants of 55 for anatase TiO₂ and 10 for both p - and n -CuInS₂, a total thickness of ~ 130 nm for the complete CuInS₂ layer is obtained in both models A and B. Furthermore, a 100 nm thick n -CuInS₂ layer with a donor density of 4×10^{16} cm⁻³ at 400 K in combination with a 30 nm thick p -CuInS₂ layer with an acceptor density of 2×10^{17} cm⁻³ at 400 K is found for model A. Model B leads to a 40 nm n -CuInS₂ film with a donor density of 2×10^{17} cm⁻³ and a 90 nm p -CuInS₂ layer with an acceptor density of 4×10^{16} cm⁻³ at 400 K. Because we initially deposited Cu-rich p -type CuInS₂, we are drawn to conclude that model B holds, meaning that the p -CuInS₂ film reaches full depletion before the n -CuInS₂ film does. A film thickness of 40 nm for the n -type region is in excellent agreement with the findings of Köttschau and Schock,³³ who observed a Cu-depleted surface layer of 5–60 nm in CuInSe₂ with grazing incidence x-ray diffraction. However, they did not report the presence of a homojunction in CuInSe₂. Although we have indications that the n -type region formed at the TiO₂/CuInS₂ interface is Cu poor as well, further investigations are in progress. Most likely, In_{Cu} will be the dominant donor in this Cu-poor n -type region.

Since in CuInS₂ both donor and acceptor states are rather deep, their ionization probability is strongly related to the temperature. Accordingly, the properties of the homo- and heterojunction change upon varying the temperature. At temperatures below 500 K, the effective donor density in TiO₂ is constant; only a small increase of the donor density around 500 K is observed. At temperatures below 400 K, the flatband situation is not reached within the applied potential range. Below 340 K, only two slopes are found, and the

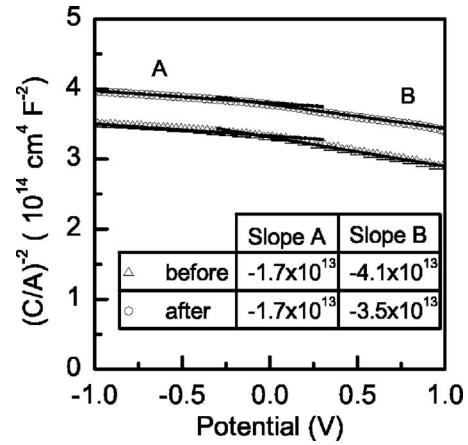


FIG. 8. C^{-2} - ϕ plots at 300 K before and after heating the sample to 500 K. In the inset, table values of both slopes A and B are given.

p -CuInS₂ film is always in full depletion within the applied potential range. A clear temperature dependence is found for donor and acceptor densities in n -CuInS₂ and p -CuInS₂, respectively, as shown in Fig. 7. It is remarkable that both acceptor and donor densities decrease with increasing temperature, opposite to our expectations. Assuming Boltzmann statistics, an activation energy of 146 meV for n -CuInS₂ is found, which is in excellent agreement with the presence of Cu_{In} acceptors.^{42,43} The fact that an acceptor is activated in n -type CuInS₂ explains the decrease in effective donor density upon increasing the temperature. In p -CuInS₂, an activation energy of 244 meV is found. For CuInS₂, this activation energy has not been reported yet. Hole traps with activation energies of 260–280 meV have been found for CuInSe₂.^{44–46} Therefore, we postulate the presence of a thermally activated hole trap located 244 meV below the valence band. Hole traps are neutral when empty and positively charged when a hole is captured.

Although the chemical nature of these hole traps cannot be inferred from our experiments, it is plausible that the oxidation of Cu⁺ to Cu²⁺ is involved. Thermal activation of a hole trap in p -CuInS₂ explains the decrease of the effective acceptor density. From the derived acceptor and donor densities, in combination with the transition points of the C^{-2} - ϕ plots, the n -type and p -type CuInS₂ film thicknesses are found to be independent of the temperature, as expected.

When heating up the samples to 500 K in nitrogen, irreversible changes may occur. To evaluate the extent of such relaxation, the experiments are repeated at room temperature after cooling down the samples from 500 K. Only small differences are observed. Figure 8 shows a shift of the capacitance in the C^{-2} - ϕ plot at 300 K before and after heating to 500 K. Despite the small decrease of the capacitance, no significant differences are observed in the slopes and the transition voltages of the plots. Nevertheless, the capacitance shift indicates a minor change in the defect structure at 500 K, which is now under investigation.

IV. CONCLUSIONS

With a detailed C^{-2} - ϕ study, we provide evidence for the presence of a p - n homojunction in CuInS₂ spatially sepa-

rated from the $\text{TiO}_2/\text{CuInS}_2$ interface. A n -type CuInS_2 layer of 40 nm with a donor density of $2 \times 10^{17} \text{ cm}^{-3}$ at 400 K is present at the $\text{TiO}_2/\text{CuInS}_2$ interface. The remaining p - CuInS_2 layer has a thickness of 90 nm and an acceptor density of $4 \times 10^{16} \text{ cm}^{-3}$ at 400 K. Both acceptor and donor densities decrease with increasing temperature, due to the presence of a Cu_{In}'' acceptor level in n - CuInS_2 and a yet unidentified thermally activated hole trap in p - CuInS_2 . Activation energies of 146 and 244 meV are found, respectively.

ACKNOWLEDGMENT

Advance Surface Technologies (Bleiswijk, The Netherlands) is acknowledged for supplying the samples.

- ¹J. A. M. AbuShama, S. Johnston, T. Moriarty, G. Teeter, K. Ramanathan, and R. Noufi, *Prog. Photovoltaics* **12**, 39 (2004).
- ²T. Glatzel, D. F. Marron, T. Schedel-Niedrig, S. Sadewasser, and M. C. Lux-Steiner, *Appl. Phys. Lett.* **81**, 2017 (2002).
- ³R. Scheer, R. Klenk, J. Klaer, and I. Luck, *Sol. Energy* **77**, 777 (2004).
- ⁴K. Ramanathan *et al.*, *Prog. Photovoltaics* **11**, 225 (2003).
- ⁵M. I. Alonso, K. Wakita, J. Pascual, M. Garriga, and N. Yamamoto, *Phys. Rev. B* **63**, 075203 (2001).
- ⁶R. Klenk, J. Klaer, R. Scheer, M. C. Lux-Steiner, I. Luck, N. Meyer, and U. Rühle, *Thin Solid Films* **480**, 509 (2005).
- ⁷M. A. Green, K. Emery, D. L. King, Y. Hishikawa, and W. Warta, *Prog. Photovoltaics* **15**, 35 (2007).
- ⁸M. Gratzel, *Nature (London)* **414**, 338 (2001).
- ⁹M. Nanu, J. Schoonman, and A. Goossens, *Adv. Mater. (Weinheim, Ger.)* **16**, 453 (2004).
- ¹⁰B. van der Zanden, C. Joanta, H. Donker, M. Nanu, and B. Meester, *Proceedings of the 21st European Photovoltaic Solar Energy Conference, Dresden, Germany*, 267 (2007).
- ¹¹R. Herberholz *et al.*, *Eur. Phys. J.: Appl. Phys.* **6**, 131 (1999).
- ¹²L. Chernyak, K. Gartsman, D. Cahen, and O. M. Stafsudd, *J. Phys. Chem. Solids* **56**, 1165 (1995).
- ¹³L. L. Kerr, S. S. Li, S. W. Johnston, T. J. Anderson, O. D. Crisalle, W. K. Kim, J. Abushama, and R. N. Noufi, *Solid-State Electron.* **48**, 1579 (2004).
- ¹⁴M. Nanu, L. Reijnen, B. Meester, J. Schoonman, and A. Goossens, *Chem. Vap. Deposition* **10**, 45 (2004).
- ¹⁵M. Nanu, L. Reijnen, B. Meester, A. Goossens, and J. Schoonman, *Thin Solid Films* **431**, 492 (2003).
- ¹⁶B. Tell, J. L. Shay, and H. M. Kasper, *J. Appl. Phys.* **43**, 2469 (1972).
- ¹⁷J. Parkes, R. D. Tomlinso, and M. J. Hampshire, *J. Cryst. Growth* **20**, 315 (1973).
- ¹⁸J. Parkes, R. D. Tomlinso, and M. J. Hampshire, *Solid-State Electron.* **16**, 773 (1973).
- ¹⁹R. D. Tomlinson, E. Elliott, J. Parkes, and M. J. Hampshire, *Appl. Phys. Lett.* **26**, 383 (1975).
- ²⁰P. Migliora, B. Tell, J. L. Shay, and H. M. Kasper, *Appl. Phys. Lett.* **24**, 227 (1974).
- ²¹P. W. Yu, Y. S. Park, S. P. Faile, and J. E. Ehret, *Appl. Phys. Lett.* **26**, 717 (1975).
- ²²B. Tell, S. Wagner, and P. M. Bridenbaugh, *Appl. Phys. Lett.* **28**, 454 (1976).
- ²³S. Wagner, J. L. Shay, P. Migliora, and H. M. Kasper, *Appl. Phys. Lett.* **25**, 434 (1974).
- ²⁴P. W. Yu, S. P. Faile, and Y. S. Park, *Appl. Phys. Lett.* **26**, 384 (1975).
- ²⁵B. Tell and P. M. Bridenbaugh, *J. Appl. Phys.* **48**, 2477 (1977).
- ²⁶R. K. Ahrenkiel, L. L. Kazmerski, R. J. Matson, C. Osterwald, T. P. Masopust, R. A. Mickelsen, and W. S. Chen, *Appl. Phys. Lett.* **43**, 658 (1983).
- ²⁷L. L. Kazmerski, O. Jamjoum, P. J. Ireland, R. A. Mickelsen, and W. S. Chen, *J. Vac. Sci. Technol.* **21**, 486 (1982).
- ²⁸L. L. Kazmerski, *Thin Solid Films* **57**, 99 (1979).
- ²⁹R. Matson, R. Noufi, R. K. Ahrenkiel, R. C. Powell, and D. Cahen, *Sol. Cells* **16**, 495 (1986).
- ³⁰R. Matson, R. Noufi, K. J. Bachmann, and D. Cahen, *Appl. Phys. Lett.* **50**, 158 (1987).
- ³¹D. Schmid, M. Ruckh, and H. W. Schock, *Appl. Surf. Sci.* **103**, 409 (1996).
- ³²D. Schmid, M. Ruckh, F. Grunwald, and H. W. Schock, *J. Appl. Phys.* **73**, 2902 (1993).
- ³³I. M. Kotschau and H. W. Schock, *J. Phys. Chem. Solids* **64**, 1559 (2003).
- ³⁴Y. Yan, K. M. Jones, J. Abushama, M. Young, S. Asher, M. M. Al Jassim, and R. Noufi, *Appl. Phys. Lett.* **81**, 1008 (2002).
- ³⁵D. Cahen, J. M. Gilet, C. Schmitz, L. Chernyak, K. Gartsman, and A. Jakubowicz, *Science* **258**, 271 (1992).
- ³⁶S. Richter, Y. Manassen, and D. Cahen, *Phys. Rev. B* **59**, 10877 (1999).
- ³⁷M. Krunks, V. Mikli, O. Bijakina, and E. Mellikov, *Appl. Surf. Sci.* **142**, 356 (1999).
- ³⁸L. Kavan and M. Gratzel, *Electrochim. Acta* **40**, 643 (1995).
- ³⁹See EPAPS Document No. E-JAPIAU-102-120714 for a table with all transition voltages and slopes of the C^{-2} - ϕ measurements and the mathematical analysis of the capacitance of the four situations shown in Fig. 6. This document can be reached through a direct link in the online article's HTML reference section or via the EPAPS homepage (<http://www.aip.org/pubservs/epaps.html>).
- ⁴⁰M. Kleinfeld and H. D. Wiemhofer, *Solid State Ionics* **28**, 1111 (1988).
- ⁴¹M. Kleinfeld and H. D. Wiemhofer, *Ber. Bunsenges. Phys. Chem.* **90**, 711 (1986).
- ⁴²J. J. M. Binsma, L. J. Giling, and J. Bloem, *J. Lumin.* **27**, 35 (1982).
- ⁴³M. Nanu, F. Boulch, J. Schoonman, and A. Goossens, *Appl. Phys. Lett.* **87** (2005).
- ⁴⁴R. Herberholz, M. Igalson, and H. W. Schock, *J. Appl. Phys.* **83**, 318 (1998).
- ⁴⁵M. Igalson and H. W. Schock, *J. Appl. Phys.* **80**, 5765 (1996).
- ⁴⁶T. Walter, R. Herberholz, and H. W. Schock, *Solid State Phenom. (Polycrystalline Semiconductors IV)*, **51-52**, 309 (1996).